NANO LETTERS
Cite This: Nano Lett. XXXX, XXX, XXX−XXX
Letter
pubs.acs.org/NanoLett

Long-Range Self-Assembly via the Mutual Lorentz Force of Plasmon Radiation

Haojie Ji,[†] Jacob Trevino,[‡,§,∥] Raymond Tu,[∥,⊥] Ellen Knapp,[⊥] James McQuade,[†] Vitaliy Yurkiv,[#] Farzad Mashayek,[#] and Luat T. Vuong*[,†,‡,∥]

[†]Department of Physics, Queens College of the City University of New York, Flushing, New York 11367, United States
[‡]Department of Physics, The Graduate Center of the City University of New York, New York, New York 10016, United States
[§]Department of Chemistry, The Graduate Center of the City University of New York, New York, New York 10016, United States
[∥]Advanced Science Research Center of the Graduate Center at the City University of New York, New York, New York 10031, United States
[⊥]Department of Chemical Engineering, City College of New York, New York, New York 10031, United States
[#]Department of Mechanical and Industrial Engineering, University of Illinois at Chicago, Chicago, Illinois 60607, United States

Supporting Information

ABSTRACT: Long-range interactions often proceed as a sequence of hopping through intermediate, statistically favored events. Here, we demonstrate predictable mechanical dynamics of particles that arise from the Lorentz force between plasmons. Even if the radiation is weak, the nonconservative Lorentz force produces stable locations perpendicular to the plasmon oscillation; over time, distinct patterns emerge. Experimentally, linearly polarized light illumination leads to the formation of 80 nm diameter Au nanoparticle chains, perpendicularly aligned, with lengths that are orders of magnitude greater than their plasmon near-field interaction. There is a critical intensity threshold and optimal concentration for observing self-assembly.

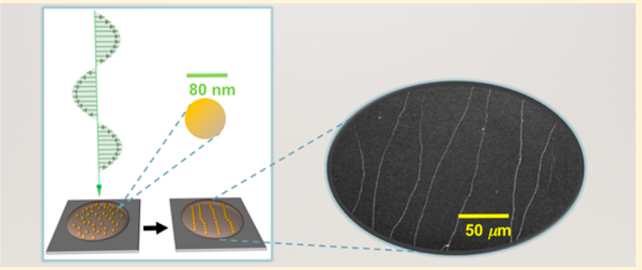

KEYWORDS: *Nanoparticle, self-assembly, plasmon, Lorentz force*

Scientists are actively studying "hot electron" dynamics and modeling the physical mechanisms that couple plasmons with each other and their environment.[1−4] The collective presence of plasmons also carries mechanical consequences that are related and significant. Plasmonic nanoparticles (NPs) have been shown to exhibit erratic light-induced motion, to be difficult to trap optically, and to settle in different equilibrium orientations when illuminated with polarized light.[5−11] Plasmon-induced motion may originate from different channels of plasmon decay; because plasmon decay produces heat and shifts electrochemical potentials, while any corresponding motion, in turn, may alter the plasmon excitation, plasmon-induced mechanical dynamics are complex. In addition, although the energy of plasmons is successfully channeled into myriad nanostructuring processes,[12−16] the plasmon decay dynamics are difficult to predict, and subsequently, the most widespread methods for self-assembling, patterning, and optically trapping metal nanostructures avoid the plasmon excitation.[17] Predictive control of plasmon dynamics, that is, the knowledge to model, a priori, the mechanical behavior of plasmonic materials in the presence of plasmons, would aid the large-area nanomanufacturing of hybrid materials and advance other photonic technologies.

Here we revisit the contribution of the radiation from plasmons, which is generally considered to be insignificant in comparison to the strong near-field response. We find that even if the radiation is weak, the corresponding Lorentz force points to locations where NPs tend to settle and minimize their energy. Over time, even in the presence of noise statistically favored events would influence longer-range spatial dynamics. We show that with mutual Lorentz interactions, the force arising between radiated fields and other plasmons, each NP experiences torque, attraction or repulsion. The calculation of the mutual Lorentz force predicts that NPs with dipole−dipole interactions would form chains in a direction perpendicular to the linear polarization of light and may explain other distinct, polarization-dependent mechanical dynamics.

Our results show that the mutual Lorentz force leads to longer-range interactions that are orders of magnitude greater than previously expected. Laser-illuminated gold NPs on indium tin oxide-coated (ITO) substrates exhibit NP chain-formations as long as 200 μm, aligned in a direction perpendicular to the polarization of the illuminating laser. Concentration-dependent regimes and intensity-dependent thresholds for self-assembly arise because there is competition

Received: January 20, 2018
Revised: March 20, 2018
Published: March 27, 2018

DOI: 10.1021/acs.nanolett.8b00269
Nano Lett. XXXX, XXX, XXX−XXX

between mutual Lorentz, gradient, and Brownian forces. The mutual Lorentz interactions between conducting NPs are not a conventional scattering or gradient force and are not generally under consideration;[18,19] however, our results are consistent with prior studies[20−23] and explain recent experimental observations of the perpendicular alignment of NPs. The understanding provided here of the longer-range time-averaged forces may demystify other self-assembling and optical trapping processes of NPs and aid our interrogation of the electrical and chemical potentials that interact with and shift with the plasmon resonance.

Results. We consider the mutual Lorentz force, the net forces between two oscillating dipoles p_1 and p_2 positioned in the $x-y$ plane where the dipoles are illuminated with a uniform plane wave traveling in the z-direction at the plasmon-resonant frequency. The dipoles carry uniform strength and equal frequency, and oscillate virtually in-phase with each other and the illuminating electric field [Figure 1a]. Prior work has

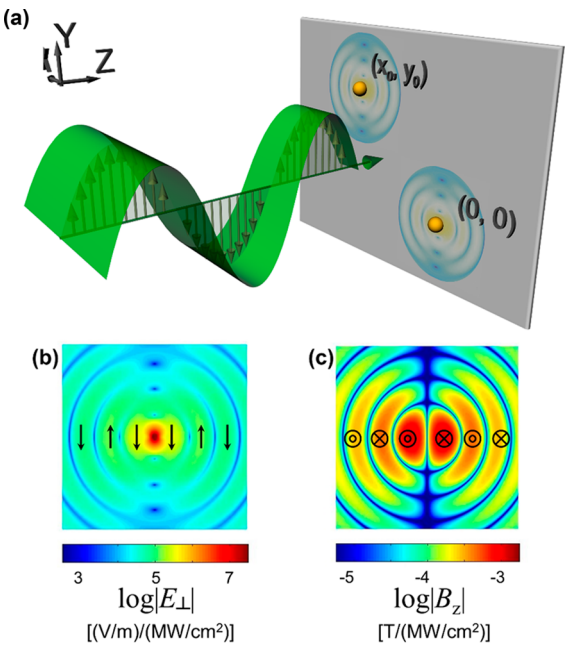

Figure 1. (a) General schematic describing Lorentz forces via dipole interactions: a plane wave with wavelength λ = 532 nm illuminates two in-phase oscillating dipoles whose displacement is (x_0, y_0). Each dipole radiates (b) electric E_r and (c) magnetic B_r fields in the $x-y$ plane, shown for a 2-μm-length area. The color plots show the real part of the time-harmonic fields on a logarithmic scale.

scrutinized the interaction where the plasmon fields of the two NPs overlap strongly[24,25] and where the distances between NPs are comparable to their diameter; in these cases, the attractive interaction between NP dimers is largely due a gradient force of the plasmon evanescent fields. We now consider the longer-distance interactions that arise from the fields radiated from each NP. Dipole p_1 produces an electromagnetic field that influences the other dipole p_2 and vice versa.

The mutual Lorentz force $F_{12} = F_{21}$ between two NPs with dipoles p_1 and p_2 is calculated

$$F_{12} = (p_2 \cdot \nabla) E_{r1} + \frac{dp_2}{dt} \times B_{r1} \quad (1)$$

where E_{r1} and B_{r1} are the radiated electric and magnetic fields from p_1 [as illustrated in Figure 1b,c] and all three terms, p, E, and B, oscillate as a function of time. The Lorentz interaction between a time-harmonic field and a dipole oscillation yields a nonzero time-averaged force, which is most commonly associated with the incident, illuminating light. It is well-known that NPs are mechanically trapped via the Lorentz force from incident-light intensity gradients[20−22,26] but when gradient forces vanish under uniform light illumination, the mutual Lorentz force associated with plasmon radiation, which we study here, is significant.

The time-averaged mutual Lorentz force is illustrated in Figure 2a (see Supporting Information for the derivation); the direction and strength of the force at each dipole depends strongly on the fields at their relative positions. For 80 nm gold NPs, we estimate that the mutual Lorentz force is, at distances comparable to a wavelength, on the order of pN for 10 MW/cm^2 illumination intensities. This result indicates that most pulsed lasers produce mutual Lorentz forces between plasmonic NPs that are on the order of the gradient forces that are conventionally leveraged for optical trapping.

The magnitude of the time-averaged Lorentz force decreases with $1/r^4$ in the near field and $1/r$ in the far field and is on the order of pN/(MW/cm^2) at distances comparable to a wavelength from the NP, which is significant for the NP interaction. One particularly important and unintuitive characteristic of the vector field of this force: unlike the Coulomb interaction between electrostatic charges, the Lorentz force is not a conservative, "central" force and is not simply either attractive or repulsive; instead, Figure 2a shows that the time-averaged mutual Lorentz force between oscillating dipoles may provide a torque between the dipoles. This feature is particularly unintuitive because the radiation momentum or Poynting of the radiated-field is directed radially outward from each oscillating dipole. The mutual Lorentz force pushes NPs toward the x-axis, in agreement with ref 23. In the near-field, the mutual Lorentz force is repulsive but weaker than the gradient force, which leads to the net attraction of NPs (see Supporting Information for quantitative comparison).

The sum of the near-field gradient force and mutual Lorentz force produces two types of stable attractors for pairs of NPs in the $x-y$ plane [Figure 2b]. One of the stable attractors consists of pairs of adjacent NPs or dimers, pinned by a net attractive force and aligned perpendicular to the dipole oscillation or polarization (on the x-axis for y-polarized linear illumination). The other stationary attractor for the NPs, also predicted in ref 23., consists of NPs spaced at integer-wavelength distances (again, on the x-axis for y-polarized linear illumination). Stable nodes appear at integer-wavelength separations and at these locations, the Lorentz force is directed inward toward the nodes. The periodic forces along the x-axis can be viewed in a manner analogous to the Lorentz forces arising from electrical currents on parallel wires, which are either attractive or repulsive depending on whether the currents are aligned or opposed. Here, the direction of the force, either attractive or repulsive, is determined by the retarded phase of the radiated fields from adjacent NPs; the phase corresponds to the NP spacing. The resultant stable positions may have been observed in ref 27 with plasmonic NPs in an optical trap.

In a real NP system, Brownian forces are present. Despite noise, over time NPs move toward stable positions with lower energy. These new stable positions would tend to be stable nodes that are closer or adjacent to other NPs since the mutual Lorentz force and the gradient force both increase with smaller NP separation [Figures 2b and S2]. The calculation of the

DOI: 10.1021/acs.nanolett.8b00269
Nano Lett. XXXX, XXX, XXX−XXX

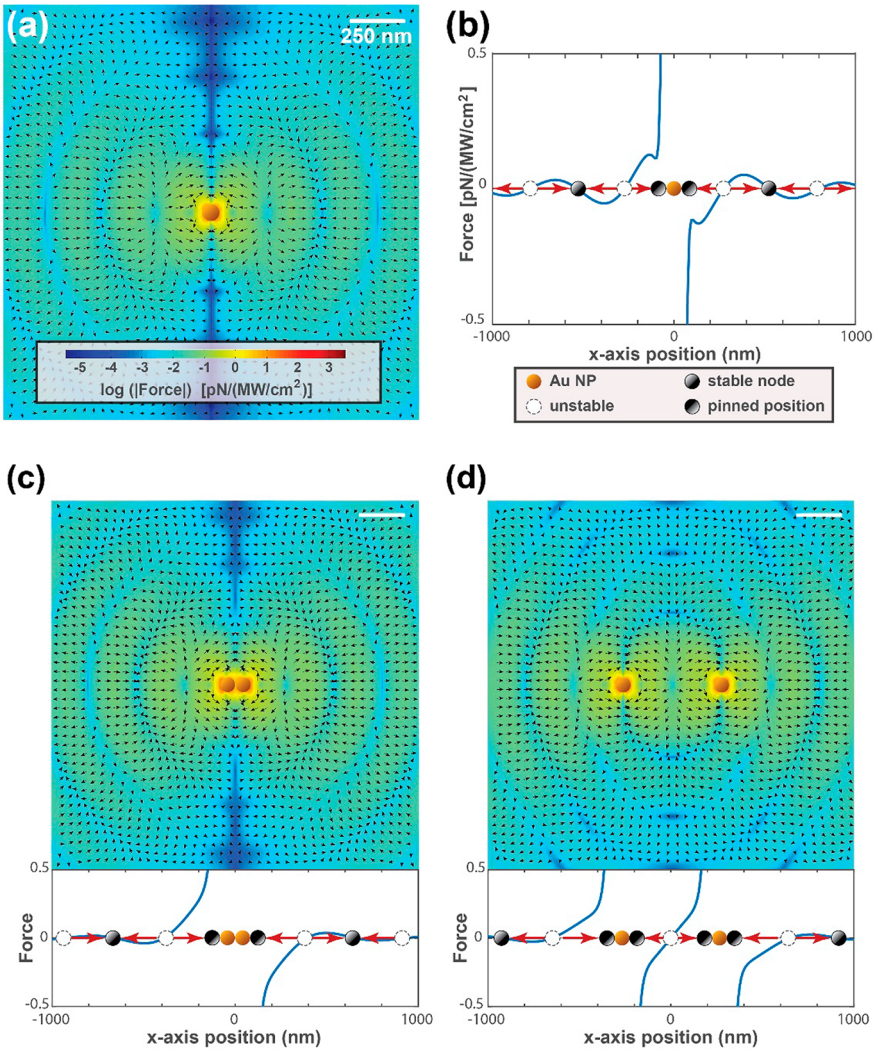

Figure 2. (a) Vector field showing the time-averaged mutual Lorentz force $F_{12}(x_0, y_0)$ at an oscillating dipole positioned at (x_0, y_0) as a result of the dipole radiation from a nanoparticle (NP) at the origin. Calculations assume 532 nm-wavelength, vertically polarized (y-direction) excitation and induced dipole from an 80 nm Au NP. (b) The corresponding stable, unstable, and stably pinned positions on the x-axis as a result the gradient and mutual Lorentz forces. There is no vertical component; the force is pointed to right (left) if positive (negative). Similar vector-field plots of the mutual Lorentz force [above] and plot of the x-axis stable points [below] resulting from (c) 2 adjacent NPs and (d) 2 NPs separated by 532 nm on the x-axis.

Lorentz force is subsequently extended to consider the superposition of two adjacent, or one-wavelength separated, NP dipoles [Figure 2c,d]. The vector flow of the forces and the presence of pinned positions and stable nodes on x-axis [Figure 2c,d] explain the subsequent one-dimensional (1D) alignments of NPs, which are reported in previous efforts,[15,16,28] and observed in our own experiments. We expect that when multiple NPs are aligned along the x-axis, the total energy is significantly lower.

In comparison to prior studies that have scrutinized the mechanical forces between plasmonic NPs, our results indicate that far-field effects contribute to the evolved system dynamics. At near-field distances,[24,25] gradient forces[27] and thermal responses[29,30] influence the motion of NPs. In general, NPs align either parallel or perpendicular to the illuminating laser polarization as a result of the attractive near-field dimer interactions of spherical NPs. In contrast, NPs experience torque and settle at stable nodes as a result of the mutual Lorentz force. These distinct signatures agree with the far-field-region behavior discussed in ref 23. The effect of the pattern formation, that is, the perpendicular alignment and formation of NP chains, is experimentally observed to be more dramatic than would be predicted by calculation of the mutual Lorentz force, alone. The sequential, NP hopping from stable node to stable node or pinned position leads to the long-range spatial dynamics.

Figure 3a shows the schematic experimental setup and Figure 3b–e shows the SEM images of the NP drop-cast samples at different concentrations where the laser pulse peak intensities are 20 MW/cm^2. Here, gold NPs settle on ITO-coated substrates under pulsed-laser illumination at the plasmonic resonance of 532 nm. Images are taken toward the center of the drops. The samples that are prepared without laser light and the samples prepared with circularly polarized 532 nm laser light do not exhibit any patterns [Figure 3b,c]; by contrast, the settled Au NP samples prepared with linearly polarized 532 nm laser light exhibit distinct string formations [Figure 3d,e]. With linearly polarized 1060 nm (off resonant) laser light, no patterns are observed [not shown]. Alignment errors of ±15° may be attributed to variations of the laser polarization or

DOI: 10.1021/acs.nanolett.8b00269
Nano Lett. XXXX, XXX, XXX−XXX

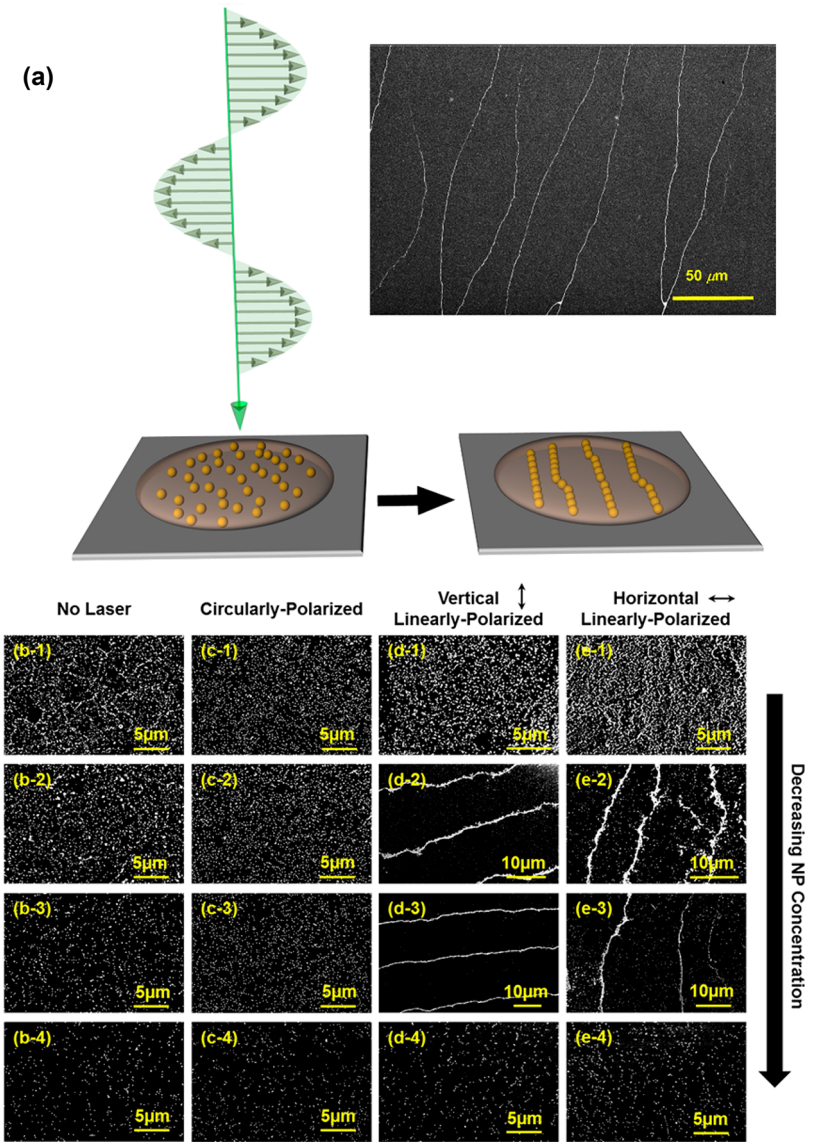

Figure 3. (a) Schematic diagram of NP drop under illumination of linearly polarized laser, and the SEM image of the string pattern of NPs. (b–e) SEM images of samples prepared (b) without laser (c) with circularly polarized (d) vertical linearly polarized and (e) horizontal linearly polarized laser with NP concentrations (1) 0.0500 mg/mL, (2) 0.0375 mg/mL, (3) 0.0250 mg/mL, and (4) 0.0125 mg/mL. The laser has wavelength λ = 532 nm and peak laser intensity I_{max} = 20MW/cm^2.

Poynting axis, deviations in sample preparation or sample alignment in the SEM. We calculate NP area densities (NPs/μm^2) by analyzing the SEM images in MATLAB.

The presence of the self-aligned patterns only appears under the illumination of linearly polarized laser light at the resonant frequency in regions of moderate NP area densities (6–16 NPs/μm^2). The chains of NPs are tilted but generally aligned perpendicular to the direction of the laser polarization. The perpendicular alignment to the linear polarization of the light is the signature of the mutual Lorentz force of the dipole excitation. The perpendicularly aligned chains are independent of the orientation of the substrate. Hydrodynamic effects, such as thermophoresis, evaporation, and convection,[31,32] which have also been shown to lead to self-assembly (e.g., coffee ring[32]), are moderately suppressed in our system where the drying occurs on a hydrophilic surface and where laser light illuminates the entire drop (see Methods and Materials and Supporting Information for additional details). Hydrodynamic effects are largely independent of the light polarization, so that they cannot be the origin of the self-assembled chains that are always perpendicular to the laser linear polarization.

In general, the structure of the line patterns depends on the area density of the NPs. In regions where the area density is 1–3 NP/μm^2, short scattered lines are observed. These NP segments are less than 10 μm in length but are interspersed uniformly. At area densities of 6–16 NP/μm^2 distinct patterns consisting of long parallel lines (>100 μm) are observed, as shown in Figure 3d,e. When the area density is higher, these longer NP strands appear more zigzagged. At the highest NP densities, heating, surface functionalization, and gradient-force attraction lead to the formation of blocks.[33] If the NP density is low (<1 NP/μm^2), then individually dispersed NPs are observed, and we infer that the Lorentz forces are too small to overcome the randomly directed forces associated with Brownian motion.

DOI: 10.1021/acs.nanolett.8b00269
Nano Lett. XXXX, XXX, XXX–XXX

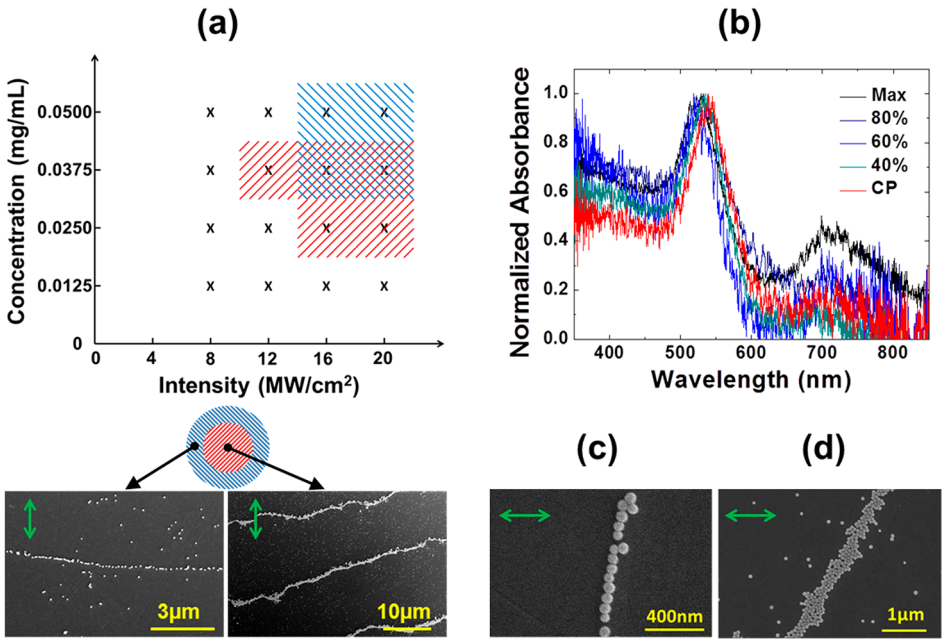

Figure 4. (a) Phase diagram of the Au NP self-assembly, which is observed as long parallel lines in the central region (red lines) and scattered short lines in outside region (blue lines), as shown at the bottom, inset. (b) Normalized absorbance of samples prepared with 0.0375 mg/mL concentration (11−16 NP/μm^2): samples are illuminated by linearly polarized laser light at a range of intensities (8−20 MW/cm^2) and circularly polarized laser light at the maximum intensity (20 MW/cm^2). (c,d) Magnified SEM images of NP thin and thick strings, respectively. The green double arrows represent the direction of the laser linear polarization.

Strong solvent−substrate interactions are observed and are considered essential to the stability of the formed patterns.[34] Evidence of the substrate−solvent interactions is the presence of a distinct colloidal coffee ring, a diameter that identifies "pinning" of the initial droplet base[35] [See Figure S1b] that is marked by stacked Au NPs. The colloidal coffee ring that arises from evaporation and convection appears isotropic and its self-assembled patterns are independent of the polarization of laser. We expect that the primary role of the substrate is to suppress the Brownian motion.[36,37] In bulk NP solution, we measure the diffusion coefficient $D = 1.6 \times 10^{-12}$ m^2/s via dynamic light scattering, and the equivalent force is expected to be orders of magnitude larger than the mutual Lorentz force calculated here. In other words, we anticipate that in bulk solution, Brownian forces arrest the long-range pattern formation.

We also anticipate that electrostatic interactions between the substrate and sample have a strong role in promoting self-assembly. The substrate electrostatic interactions may change the effective NP ζ-potential (measured to be −17 eV). Where NPs aggregate into blocks or form thick lines on the substrate, the NPs settle in a (single) monolayer, as shown via the magnified SEM images (Figure 4c,d). The assembling process appears to commence after an initial group of NPs have been pinned to the substrate. To confirm this, we prepare samples with which we block the laser (linearly polarized 532 nm) at a time interval of 2 min before the solution drop is completely dry. As expected, we observe no line patterns in the majority of these samples; those chains that do form manifest to a much lower degree. From this we conclude that the majority of the NP chains are formed during the last 1 or 2 min of drying.

We build a phase diagram that illustrates the pattern formation produced by varying illumination intensities and NP concentrations [Figure 4a]; we find that the phase plot varies depending on the imaged location of the drop (i.e., inside/outside the coffee ring). Experimentally, we observe both lower and upper NP-concentration thresholds for the self-aligned patterns, and we only observe a lower critical intensity threshold. With an intensity of 12 MW/cm^2, the ideal NP concentration is 0.0375 mg/mL, which corresponds to area densities of 11−16 NP/μm^2. The pattern formation only occurs at finite concentrations because the mutual Lorentz force competes with gradient and Brownian forces.

The degree of pattern formation increases with intensity; the NP self-alignment is observed over smaller areas in the droplet at lower intensity; as the intensity increases, the NP patterns are observed across larger areas of the drop. Figure 4b shows the absorbance spectra from 0.0375 mg/mL NP samples prepared with various illuminating laser intensities and polarizations. The absorbance spectra of the samples with the largest NP self-assembly show extra peaks at wavelengths of λ = 700 nm; the prominence of the 700 nm peak corresponds with the completion of NP self-assembly and is associated with the resonance of 1D Au NP arrays or dimers.[38] From the relative intensity of the ∼700 nm band and SEM sample scans, we estimate that at most 30% of the NPs are self-assembled into strings, and this ratio decreases with decreasing illumination intensity.

We generalize that the long-range self-assembly mechanism of the NPs under resonant illumination occurs as follows. Initially NP chains are seeded by a dimer or a pair of attracted NPs. This dimer formation occurs uniformly throughout the sample, rather than at nucleation sites at the boundary of the sample. The NPs both settle at stable nodes produced by the mutual Lorentz force and also produce stable nodes via their radiation, migrating toward more stable positions that minimize the energy of the system. The NPs align perpendicular to the polarization and generally grow toward other self-assembled NPs that are also aligned on-axis. As the density of aligned NPs increases, attractive gradient forces connect nearby NPs and lead to the formation of connected chains [as shown in Figure

DOI: 10.1021/acs.nanolett.8b00269
Nano Lett. XXXX, XXX, XXX−XXX

4c,d]. As NP patterns grow, they produce stronger dipole interaction forces, extending influence to other nearby NPs, which also align perpendicular to the laser polarization as they are drawn to the self-assembled NP-chain structures [as illustrated in Figure 2c,d]. With samples prepared with high illumination intensity and higher NP densities, chains zigzag or crossover because chains connect before dimers align. This cascaded process of assembly, which leverages the intermediate configurations of stability, leads to NP chains that are orders of magnitude longer than the extent of the plasmon evanescent fields.

In conclusion, we have investigated the non-negligible time-averaged mutual Lorentz force associated with plasmon radiation. These interactions have an accumulated long-range effect on the self-assembly of plasmonic NPs, particularly when dried on a flat substrate on which thermal Brownian forces are minimized. Experimental images of NP solutions dried on ITO substrate under linearly polarized laser illumination at the plasmon resonance consistently reveal these effects. We observe a process of pattern formation that is analogous to spinodal decomposition, where disperse, aligned formations of individual dimers gradually join into longer NP strands as long as 200 μm, aligned perpendicular to the linear polarization of the illuminating laser. The longer-range responses are expected to emerge from the cascaded plasmon interactions and intermediate stable configurations dictated by the mutual Lorentz force, which is relevant to nascent models of plasmonically powered processes.

■ ASSOCIATED CONTENT

Supporting Information

The Supporting Information is available free of charge on the ACS Publications website at DOI: 10.1021/acs.nanolett.8b00269.

Models and calculations for the Lorentz forces; details regarding sample preparation and measurement procedures; detailed description of experimental observations; Table S1 of sample preparation parameters; Figure S1 of sample preparation setup; Figure S2 showing of calculated comparison of mutual Lorentz force with gradient force (PDF)

■ AUTHOR INFORMATION

Corresponding Author

*E-mail: Luat.Vuong@qc.cuny.edu.

ORCID

James McQuade: 0000-0002-1100-3990

Luat T. Vuong: 0000-0002-0652-4214

Notes

The authors declare no competing financial interest.

■ ACKNOWLEDGMENTS

L.T.V. graciously acknowledges funding from NSF DMR 1151783 and DMR 1709446. H.J. is funded via the City University Advanced Science Research Postdoctoral Collaborative Grant. This work was performed in part at the Advanced Science Research Center NanoFabrication Facility of the Graduate Center at the City University of New York. The authors acknowledge helpful discussions with Benjamin W. Stewart and Michael Mirkin.

■ REFERENCES

(1) Besteiro, L. V.; Kong, X. T.; Wang, Z. M.; Hartland, G.; Govorov, A. O. *ACS Photonics* **2017**, *4*, 2759−2781.

(2) Brongersma, M. L.; Halas, N. J.; Nordlander, P. *Nat. Nanotechnol.* **2015**, *10*, 25−34.

(3) Prodan, E.; Radloff, C.; Halas, N. J.; Nordlander, P. *Science* **2003**, *302*, 419−422.

(4) Nordlander, P.; Oubre, C.; Prodan, E.; Li, K.; Stockman, M. I. *Nano Lett.* **2004**, *4*, 899−903.

(5) Thijssen, R.; Verhagen, E.; Kippenberg, T. J.; Polman, A. *Nano Lett.* **2013**, *13*, 3293−3297.

(6) Toussaint, J. K. C.; Liu, M.; Pelton, M.; Pesic, J.; Guffey, M. J.; Guyot-Sionnest, P.; Scherer, N. F. *Opt. Express* **2007**, *15*, 12017−12029.

(7) Moocarme, M.; Kusin, B.; Vuong, L. T. *Opt. Mater. Express* **2014**, *4*, 2355−2367.

(8) Yan, Z.; Pelton, M.; Vigderman, L.; Zubarev, E. R.; Scherer, N. F. *ACS Nano* **2013**, *7*, 8794−8800.

(9) Yan, Z.; Sweet, J.; Jureller, J. E.; Guffey, M. J.; Pelton, M.; Scherer, N. F. *ACS Nano* **2012**, *6*, 8144−8155.

(10) Volpe, G.; Quidant, R.; Badenes, G.; Petrov, D. *Phys. Rev. Lett.* **2006**, *96*, 238101.

(11) Blattmann, M.; Rohrbach, A. *Nano Lett.* **2015**, *15*, 7816−7821.

(12) Jin, R. *Science* **2001**, *294*, 1901−1903.

(13) Yeom, J.; Yeom, B.; Chan, H.; Smith, K. W.; Dominguez-Medina, S.; Bahng, J.; Zhao, G.; Chang, W.-S.; Chang, S.-J.; Chuvilin, A.; Melnikau, D.; Rogach, A. L.; Zhang, P.; Link, S.; Král, P.; Kotov, N. A. *Nat. Mater.* **2015**, *14*, 66−72.

(14) Lin, L.; Peng, X.; Wang, M.; Scarabelli, L.; Mao, Z.; Liz-Marzán, L. M.; Becker, M. F.; Zheng, Y. *ACS Nano* **2016**, *10*, 9659−9668.

(15) Jin, R.; Cao, Y. C.; Hao, E.; Métraux, G. S.; Schatz, G. C.; Mirkin, C. A. *Nature* **2003**, *425*, 487−490.

(16) Stenhammar, J.; Wittkowski, R.; Marenduzzo, D.; Cates, M. E. *Sci. Adv.* **2016**, *2*, e1501850.

(17) Song, J.; Niu, G.; Chen, X. *Bioconjugate Chem.* **2017**, *28*, 105−114.

(18) Juan, M. L.; Righini, M.; Quidant, R. *Nat. Photonics* **2011**, *5*, 349−356.

(19) Dienerowitz, M.; Mazilu, M.; Dholakia, K. *J. Nanophotonics* **2008**, *2*, 021875.

(20) Paul, W. *Rev. Mod. Phys.* **1990**, *62*, 531−540.

(21) Futamata, M.; Akai, K.; Iida, C.; Akiba, N. *Anal. Sci.* **2017**, *33*, 417−426.

(22) Kemp, B. A.; Grzegorczyk, T. M.; Kong, J. A. *J. Electromagnetic Wave* **2006**, *20*, 827−839.

(23) Dholakia, K.; Zemánek, P. *Rev. Mod. Phys.* **2010**, *82*, 1767−1791.

(24) Tong, L.; Miljković, V. D.; Johansson, P.; Käll, M. *Nano Lett.* **2011**, *11*, 4505−4508.

(25) Miljković, V. D.; Pakizeh, T.; Sepulveda, B.; Johansson, P.; Käll, M. *J. Phys. Chem. C* **2010**, *114*, 7472−7479.

(26) Chaumet, P. C.; Nieto-Vesperinas, M. *Opt. Lett.* **2000**, *25*, 1065−1067.

(27) Li, Z.; Kall, M.; Xu, H. *Phys. Rev. B: Condens. Matter Mater. Phys.* **2008**, *77*, 085412.

(28) Silvera Batista, C. A.; Larson, R. G.; Kotov, N. A. *Science* **2015**, *350*, 1242477.

(29) Gargiulo, J.; Cerrota, S.; Cortés, E.; Violi, I. L.; Stefani, F. D. *Nano Lett.* **2016**, *16*, 1224−1229.

(30) Braun, M.; Cichos, F. *ACS Nano* **2013**, *7*, 11200−11208.

(31) Ming, T.; Kou, X.; Chen, H.; Wang, T.; Tam, H.-L.; Cheah, K.-W.; Chen, J.-Y.; Wang, J. *Angew. Chem., Int. Ed.* **2008**, *47*, 9685−9690.

(32) Cheng, X.; Xu, X.; Rice, S. A.; Dinner, A. R.; Cohen, I. *Proc. Natl. Acad. Sci. U. S. A.* **2012**, *109*, 63−67.

(33) González-Rubio, G.; González-Izquierdo, J.; Bañares, L.; Tardajos, G.; Rivera, A.; Altantzis, T.; Bals, S.; Peña-Rodríguez, O.; Guerrero-Martínez, A.; Liz-Marzán, L. M. *Nano Lett.* **2015**, *15*, 8282−8288.

DOI: 10.1021/acs.nanolett.8b00269
Nano Lett. XXXX, XXX, XXX−XXX

(34) Tian, X.; Zheng, H.; Mirsaidov, U. *Nanoscale* **2017**, *9*, 10044−10050.
(35) Verch, A.; Pfaff, M.; de Jonge, N. *Langmuir* **2015**, *31*, 6956−6964.
(36) Chee, S. W.; Baraissov, Z.; Loh, N. D.; Matsudaira, P. T.; Mirsaidov, U. *J. Phys. Chem. C* **2016**, *120*, 20462−20470.
(37) Zhang, Z.; Zhang, X.; Xin, Z.; Deng, M.; Wen, Y.; Song, Y. *Adv. Mater.* **2013**, *25*, 6714−6718.
(38) Lin, S.; Li, M.; Dujardin, E.; Girard, C.; Mann, S. *Adv. Mater.* **2005**, *17*, 2553−2559.

DOI: 10.1021/acs.nanolett.8b00269
Nano Lett. XXXX, XXX, XXX−XXX